AIAA JOURNAL
Vol. 36, No. 9, September 1998

Immediate and Near Wake Flow Patterns Behind Slotted Disks

Hiroshi Higuchi,* Jinzhong Zhang,† Shojiro Furuya,‡ and Brian K. Muzas§
Syracuse University, Syracuse, New York 13244-1240

The effect of spacing ratio on the near-wake regions immediately behind porous disks that consisted of multiple annular elements is investigated experimentally. Annular jets through individual slots merge into groups of high-momentum regions that displace a global recirculating region downstream. Multiple wake patterns result from the same overall conditions. Once the pattern forms, it remains nearly unchanged unless the flow is disturbed. Compared to the flow behind a solid disk, three-dimensional large-scale motions are suppressed downstream and the wake motions are more axisymmetric. The patterns of jet mergings are also axisymmetric and persistent. The mean and time-dependent large- and small-scale velocity fluctuations are characteristic of individual spacing ratios and flow patterns, and they are analyzed and compared with flow visualizations. The process of how the wake settles into a certain flow pattern also is addressed.

I. Introduction

IN an attempt to suppress the large level of wake motions behind bluff bodies, base bleed or a porous surface is often employed. The theoretical basis for global and absolute instabilities in the wake and their control is reviewed in Ref. 1. Examples of the two-dimensional wake control can be found in Ref. 1 as well as in Refs. 2 and 3. The present paper is concerned with flow past axisymmetric bluff bodies that often is encountered in engineering practice. One such bluff body is a high-performance parachute that typically undergoes a complicated wake flow–structure interaction process.[4] A considerable amount of basic research has been conducted on the characteristics of the wakes behind axisymmetric bluff bodies. We limit ourselves to the wake behind a sharp-edged body that has a clear separation line and exclude geometries such as spheres. Fuchs et al.[5] measured the vortex shedding frequencies behind a disk and conducted space–time correlations in the wake. Berger et al.[6] investigated the effects of forced disk oscillation on the wake structure. Using solid disks and screens, porosity effects were studied by Bevilaqua and Lykoudis[7] and more recently by Cannon et al.[8] The latter study was notable for its use of an axisymmetric rake consisting of eight hot-wire probes that enabled Cannon et al. to conduct modal decomposition of large-scale structures. In general, predominantly helical large-scale motions were suppressed at larger porosity, where no reverse flow was observed. Roberts[9] measured pressure distributions on the solid and slotted disks and attributed nonuniform base pressure distributions on the slotted disks to irregular mergings of jets, although no direct field measurement or flow visualizations were made.

Wakes immediately behind two-dimensional or axisymmetric slotted bluff bodies exhibit complex structures that are dominated by vortex shedding and jet merging, dependent on the specific geometries rather than overall porosity ratio. When the spacing between the elements of the body is large relative to the characteristic dimensions of the elements, the individual wakes behave independently close to the model. When spacing is small relative to the characteristic dimensions of the elements, the slotted bluff body acts almost as a single entity with regular vortex shedding. At intermediate spacings, however, irregular wake flow patterns are known to occur. This phenomenon has been demonstrated behind simple geometries such as a pair of flat plates[10] and a ring model.[11,12] The effect of the spacing ratio in two-dimensional grid models also has been studied.[13–15] In Ref. 15, delayed vortex formation and shedding were observed downstream of models at larger spacing ratios. A center opening, or vent, tended to further suppress the large wake oscillations. In the vented, small-spacing-ratio model, velocity and base pressure distribution were very asymmetric because of the deflected central jet. The asymmetric flow patterns were easily triggered to switch among themselves. The time-dependent behavior of wake vortices behind a closely spaced pair of flat plates was studied with the aid of wavelet analysis.[10] Two-dimensional and three-dimensional large-scale structures were examined behind a nominally two-dimensional porous plate.[2,3] However, detailed study of the flow structure behind axisymmetric slotted bluff bodies has not yet been conducted. It is important to study such flows and wake modifications because the wakes of simple axisymmetric models such as circular disks are known to evolve into fully three-dimensional flows.

It is the objective of the present investigation to study the effect of the slots on the wake and to compare the results with flows behind a solid disk and those behind two-dimensional grid models. Questions raised here were whether the wake behind axisymmetric geometry exhibits multiple flow patterns as in two-dimensional grid models and, if so, whether the patterns remain symmetric and are subject to transient switching of the patterns. Interactions between small-scale jet flow in the near wake and large-scale motions downstream are also examined.

II. Experimental Setup

The study was conducted in the recirculating-typelow-speed water channel at Syracuse University. The test section after the 6:1 contraction section is made of Plexiglas®, and it is 0.61 m wide, 0.61 m deep, and 2.44 m long. The free surface exists on the top.

A. Models

Three slotted disks of different spacing ratios were used in addition to a solid disk as a control. Schematics of models are shown in Fig. 1. The slotted disks all have three annular slots and a central vent whose radius equals the slot width. Spacing ratios of the three models tested are $s/h = 0.25$, 0.50, and 1.0, which correspond to geometric porosities of 15.8, 27.5, and 43.4%, respectively. The spacing ratio s/h is defined as the width s of the slots divided by the width h of the solid elements. All disk models had a diameter of 10.2 cm and were machined out of 0.084-cm-thick aluminum plate. The models were anodized to prevent corrosion.

The models were suspended in the test section using four 0.25-mm monofilament nylon wires. Chiefly because of a low Reynolds

Received May 20, 1997; presented as Paper 97-1480 at the AIAA 14th Aerodynamic Decelerator Systems Technology Conference, San Francisco, CA, June 3–5, 1997; revision received May 21, 1998; accepted for publication May 26, 1998.

*Professor, Department of Mechanical, Aerospace, and Manufacturing Engineering. Associate Fellow AIAA.

†Graduate Student, Department of Mechanical, Aerospace, and Manufacturing Engineering.

‡Visiting Scholar, Department of Mechanical, Aerospace, and Manufacturing Engineering; permanent address: Nagoya Guidance and Propulsion Systems, Mitsubishi Heavy Industries, Ltd., Komaki-Shi 485, Japan.

§NSF-REU Program Undergraduate Fellow, Department of Mechanical, Aerospace, and Manufacturing Engineering; currently Graduate Student, Graduate Aeronautical Laboratories, California Institute of Technology, Pasadena, CA 91125.

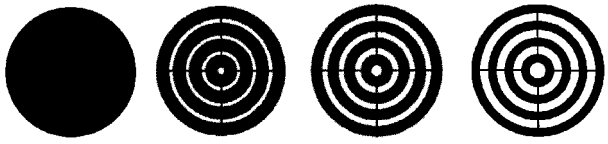

a) $s/h = 0.0$ b) $s/h = 0.25$ c) $s/h = 0.5$ d) $s/h = 1.0$

Fig. 1 Test models.

number based on the wire diameter, no adverse effect of the support was detected during the experiment. The majority of the experiments was conducted at a Reynolds number of 7.4×10^3 based on the disk diameter. Although the visualization experiments were also conducted at higher velocities, corresponding to Re up to 1.8×10^4, general features of the flow were judged unchanged.

B. Flow Visualization

The hydrogen bubble technique was employed with a horizontally placed 0.08-mm-diam platinum wire. A programmable dc power supply was connected to a function generator to produce continuous or pulsed voltage. In some instances, the electrode was connected to the model itself to produce more global hydrogen bubble generation, and the cross section of the wake parallel to the model was illuminated with a laser light sheet. Flow visualizations were recorded with a Hi8 camcorder. Video sequences subsequently were digitized with SCION Image 2000 Motion Capture card on a Macintosh Quadra computer.

C. Velocity Measurement

The mean and fluctuating velocities behind the disks were measured with a TSI two-component fiber-optic laser Doppler velocimetry (LDV) system. The fiber-optic probe, which was mounted on a three-dimensional traversing mechanism, had a diameter of 83 mm and a 350-mm focal length. A frequency shift was applied, and the signal was processed with TSI IFA 550 processors. The instantaneous axial and radial velocities were recorded at intervals between 10 and 50 ms. Data were subsampled from the original 8192 data points at each location as needed. Uncertainty in the velocity measurements in the presence of freestream turbulence was estimated to be less than $\pm 1.3\%$ of the freestream velocity (± 1 mm/s).

III. Results

A. Mean Velocity Profiles

The mean and fluctuating velocity fields were surveyed with LDV. Though not shown here, the mean velocity profile behind the solid disk was also measured, and the results agreed with previous findings. Behind the slotted disks, however, different flow patterns could emerge from the same configuration, as discussed in Sec. III.B. Therefore, the measurements were made in the preferred modes, and the flow patterns were visually monitored to ensure that they remained the same during the survey.

Figures 2a–2c show the mean velocity vector plots corresponding to the flow pattern typically encountered for each spacing ratio. Immediately behind each slotted disk, the recirculation regions are evident behind individual annuli with jets emerging through individual slots. The jet through the central vent is seen clearly in each case. Note that the center jet remains undeflected, in contrast to the vent jet behind two-dimensional slotted models at similar spacing ratios.[15] In two less porous cases, the center jets gradually lose their momentum and stagnate downstream. Thus the forward stagnation point of the global recirculation region of the wake is displaced downstream along the centerline. This point was found at about 0.7 D for $s/h = 0.25$ and at about 1.2 D for $s/h = 0.5$. At $s/h = 1$, the jets merge toward the centerline region and produce positive momentum at all locations shown in Fig. 2c. In spite of the low overall model solidity, the large reverse-flow regions reside near the outer shear layer ($r/D \approx 0.4$, $x/D < 1$). This is in contrast to the wake behind uniform screen models of similar porosity, where there was no detectable reverse flow.[8] (In principle, however, a negligibly small reverse-flow region should exist immediately behind each finite size screen element.)

The overall size and location of the reverse-flow regions obtained from the mean velocity measurement were also confirmed when

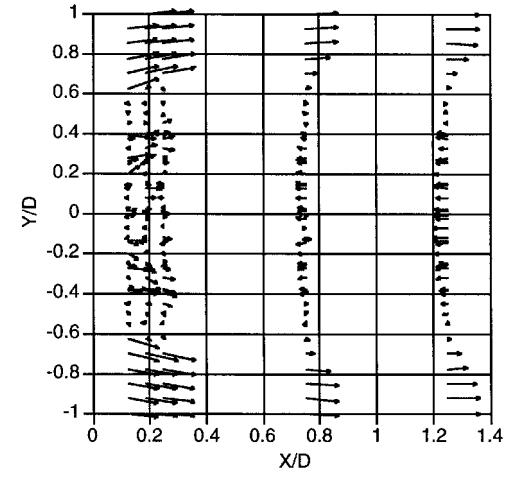

a) $s/h = 0.25$

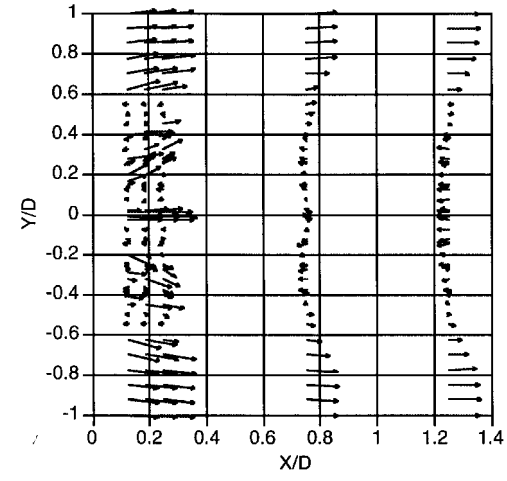

b) $s/h = 0.5$

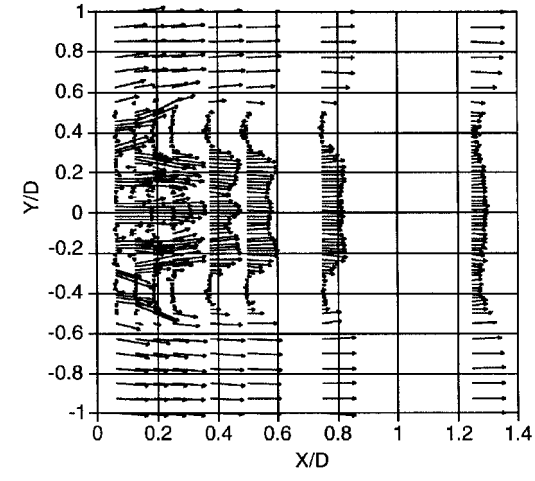

c) $s/h = 1.0$

Fig. 2 Mean velocity vector plots in the near wake.

the hydrogen bubble wire was traversed to identify the forward and rear stagnation points. For the $s/h = 0.25$ model, the reverse flow along the centerline extended from $x/D \lesssim 1.0$ to 3.0, and for the $s/h = 0.5$ case, the reverse-flow region existed from approximately $x/D = 1.2$ to 2.7. Along the centerline behind the $s/h = 1.0$ model, no reverse-flow region was found except for a small region where two (annular, to be precise) reverse-flow zones merge. The mean velocity measurements agree well with the flow visualization. Though not shown, to avoid redundancy, these velocity profiles plotted in contour forms corroborated the hydrogen flow visualizations directly. More detailed flow visualization was conducted and is shown in Sec. III.C.

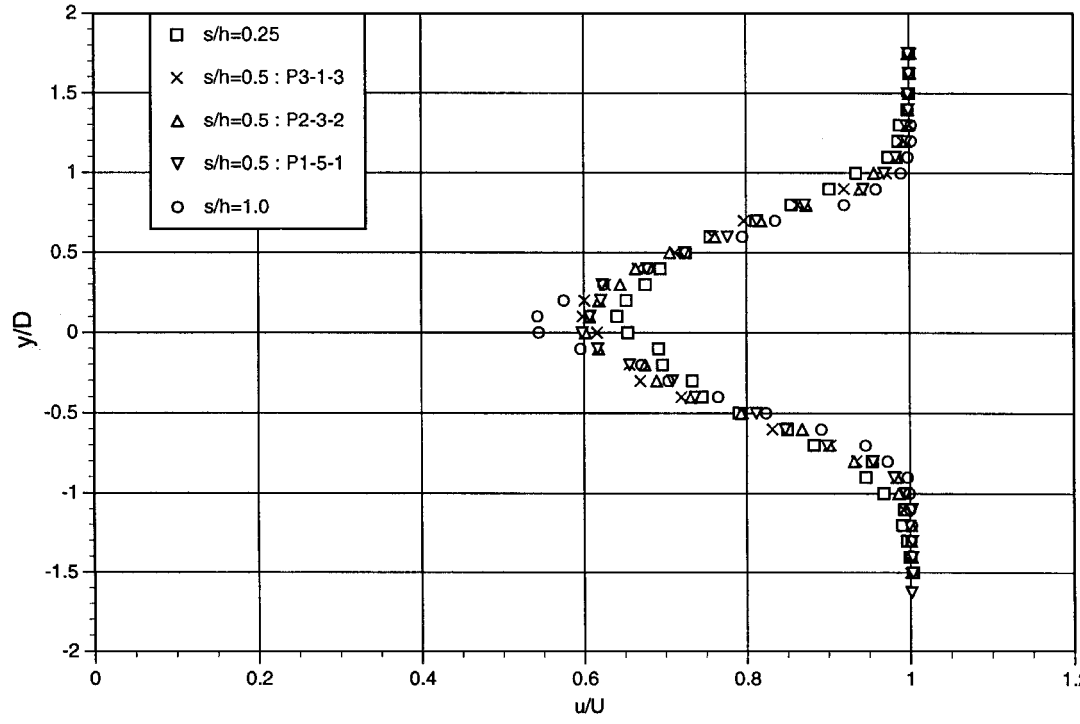

Fig. 3 Mean axial velocity profiles at $x/D = 5$.

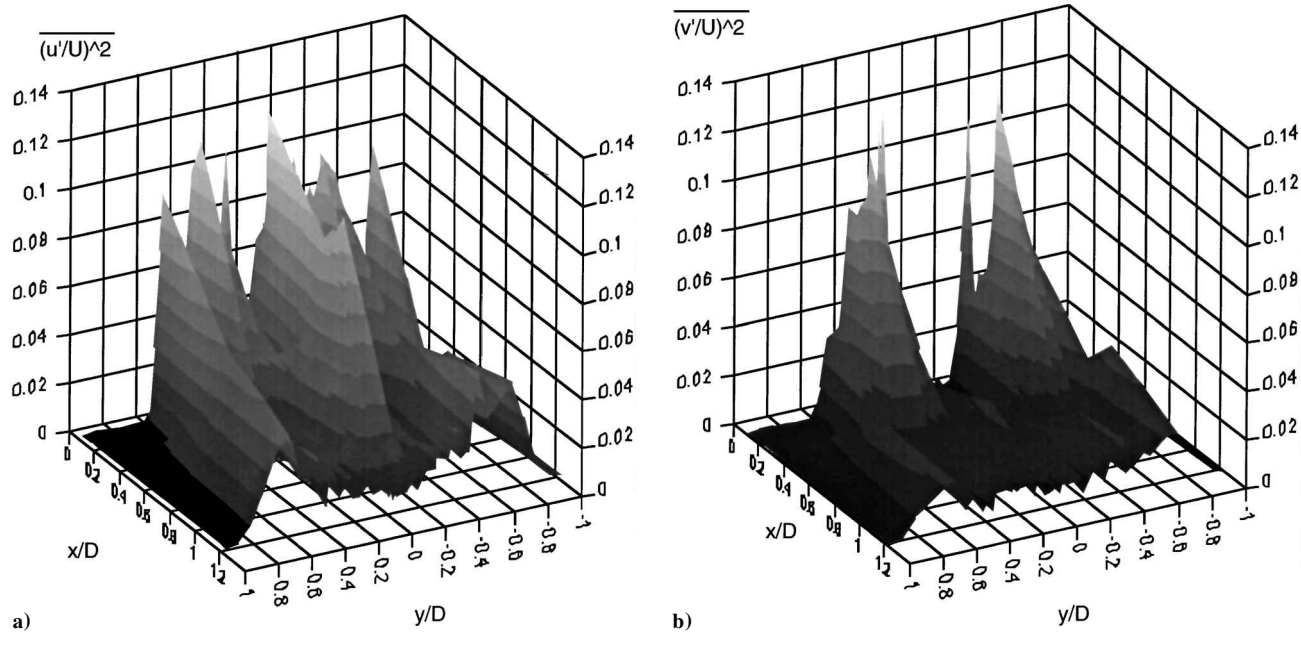

Fig. 4 Mean-squared axial and radial velocity fluctuations behind $s/h = 0.5$ slotted disk.

Farther downstream at $x/D = 5$, all of the mean velocity profiles take the form of a Gaussian profile, as shown in Fig. 3. Centerline velocity defect is the least for the highest solidity $s/h = 0.25$ case, but this is because this wake experiences the largest lateral wake oscillations. Difference among the wake widths also is noted. The intermediate spacing case is shown for different near-wake patterns discussed in Sec. III.C. The variation among the three patterns is negligible.

B. Time-Averaged Velocity Fluctuations

Instantaneous axial and radial velocity components were recorded during the wake survey. The individual jets, including the central jet, were discernible in the mean-squared axial velocity fluctuations, as shown in the $s/h = 0.5$ case in Fig. 4a. These velocity fluctuations associated with jets decay rapidly by $x/D = 1$. The radial velocity fluctuations for the $s/h = 0.25$ and 0.5 cases had strong peak(s) near 0.4–0.5 diameter from the centerline within 0.5 diameter downstream. Around $x/D = 1$, the peaks shifted outward to near 0.7 diameter from the centerline. This is particularly clear for the wake pattern labeled 3-1-3 in Sec. III.C. Figure 4b shows the radial velocity fluctuations for the $s/h = 0.5$ case. In this spacing ratio, the center jet did not manifest itself as clearly in the radial velocity fluctuations, indicating that the jet oscillations are predominantly in the axial direction. For the largest spacing ratio ($s/h = 1$), the peaks in the radial fluctuations occurred at $r/D = 0.5$, indicating a much narrower wake region than in the $s/h = 0.25$ or 0.5 cases. No two-point correlation was taken, but the hydrogen bubble flow visualization indicated that the radial flow oscillations and vortex sheddings are symmetric about the centerline at each corresponding radial position.

C. Flow Visualization Study

To further investigate characteristics of different flow patterns and the associated jet mergings and wake behavior, a flow visualization

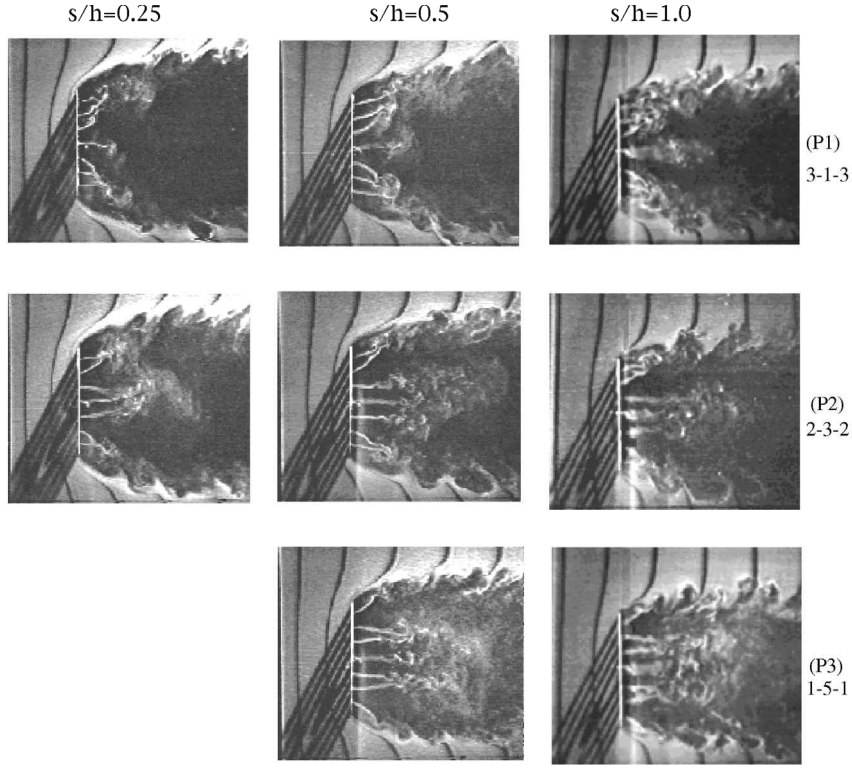

Fig. 5 Flow visualizations of near-wake patterns.

study was conducted using the hydrogen bubble technique. The results of the flow visualizations for three spacing ratios are summarized in Fig. 5. Here, the freestream velocity was 7.4 cm/s and the dc voltage was pulsed at 1.7 Hz. Between the outer shear layers of the wake, seven jets, i.e., three annular jets as well as the center jet, are visible in all cases. In addition to the outer shear-layer instability waves, small vortices are visible along individual jets. Different appearance in the wavelengths along the wake boundaries at different jet merging patterns are discussed in the next section, together with the velocity time-history analysis. In this section, our attention is focused on the global jet merging patterns. Whereas the center jet through the central vent moves downstream undeflected, annular jets are deflected strongly and merge in several different patterns. In the top group of figures labeled P1, three annular jets merge outward in the radial direction, leaving the center jet undeflected. This was the most frequently observed pattern in the $s/h = 0.25$ case. Because of the appearance of the merging jets in the two-dimensional cross section, this pattern subsequently is referred to as 3-1-3. On the other hand, the pattern in the middle row labeled P2 shows the innermost annular jet merging with the center jet, and the outer two annular jets merge and are deflected outward and interact with the outer shear layer. This is referred to as the 2-3-2 pattern. Note the symmetric merging patterns in both cases.

For the $s/h = 0.5$ case, three immediate or near-wake patterns were observed, and each had similar probability of occurrence with a slightly higher likelihood of the pattern 2-3-2, labeled P2. The top two patterns show jet merging patterns similar to those observed for $s/h = 0.25$, whereas in the additional third pattern, only the outermost annular jet is deflected outward and interacts directly with the flow past the disk edge. The other jets merge toward the center jet. This pattern is referred to as 1-5-1. Three patterns also were observed at the most porous model tested, $s/h = 1.0$. However, pattern 3-1-3 was rarely observed, whereas pattern 1-5-1 was encountered most frequently. Incidentally, pattern 1-5-1 did not occur in the $s/h = 0.25$ case.

Note the gradual shift in frequently observed patterns in Fig. 5 (diagonally from the upper left photo to the lower right photo) as the spacing ratio was increased, from solid disk-like pattern 3-1-3 to base-bleed flow pattern 1-5-1.

All of the flow patterns were persistent: Once a particular flow pattern was established, no changes in wake structure occurred in the absence of a disturbance. Change in wake patterns could be triggered by 1) turning the water channel off and on or 2) momentarily disturbing the flow with a turbulence-generating screen upstream of the model. (A grid of 25-cm diam produced approximately 14% turbulence.) Comparatively speaking, the three patterns for the $s/h = 0.5$ cases were easier to trigger into another in the group. Interestingly, transient behavior between the patterns was also axisymmetric. The mean velocity vector plots in Figs. 2a–2c correspond to patterns 3-1-3, 3-1-3, and 2-3-2, respectively, at three spacing ratios.

Farther downstream, $5 < X/D < 20$, the flow visualizations showed increased three-dimensional large-scale motions with smaller spacing ratios, which are addressed further in Sec. IV.A.

D. Wavelet and Spectral Analysis

The velocity fluctuations measured for each model were analyzed using wavelet and spectral analysis. The velocity fluctuations were recorded at two axial locations ($x/D = 0.5$ and 5). The radial positions were all at $r/D = 0.7$ with the two following exceptions at the $x/D = 0.5$ station: $r/D = 0.8$ for the solid disk and $r/D = 0.75$ for the slotted disk with $s/h = 0.25$. These adjustments were made to keep measurement points outside the recirculation region.

The wavelet analysis has been found to be a useful tool in studying unsteady, nonperiodic flowfields with intermittent multiple-scale events. It was applied to the wake interaction problem behind two flat plates,[10] where vortices from the deflected jet interacted with the outer shear-layer vortices in a way similar to the present problem. The g_2 (Mexican hat) wavelet transform was employed as in the earlier paper.[10] The time-frequency map of wavelet transform shown in Figs. 6–9 is normalized by the individual amplitude range and is represented by 15 contour levels with equal increment. The dashed contour lines indicate negative levels, and the solid lines indicate positive levels. The power spectral density is normalized by the total energy of the signal.

1. *Effects of Spacing Ratio*

To address the spacing ratio effects on the flow characteristic behind various models, the most stable (likely to occur) patterns for each spacing ratio were chosen. The wavelet transforms and power spectra of the axial velocity traces in the immediate wake $x/D = 0.5$ for three different models are shown in Fig. 6, and those

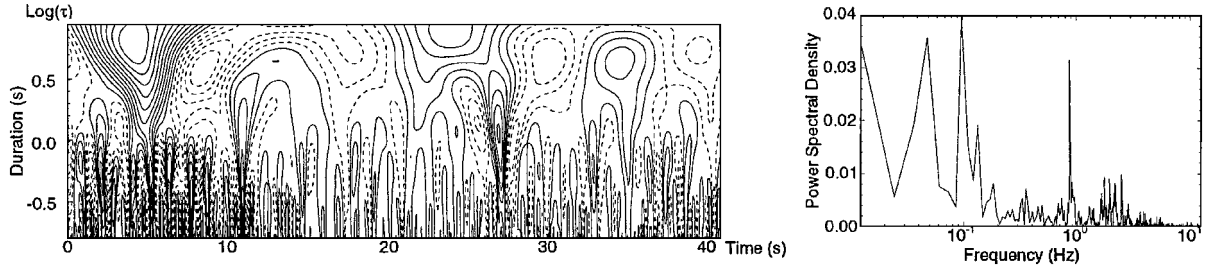

a) Solid disk, $r/D = 0.8$

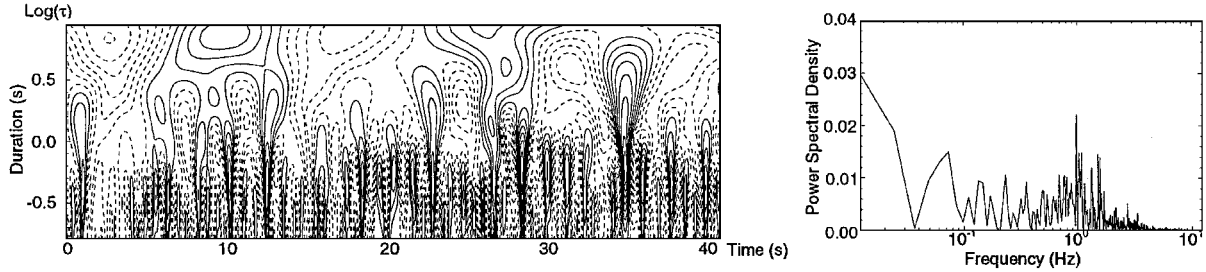

b) $s/h = 0.25, r/D = 0.75$

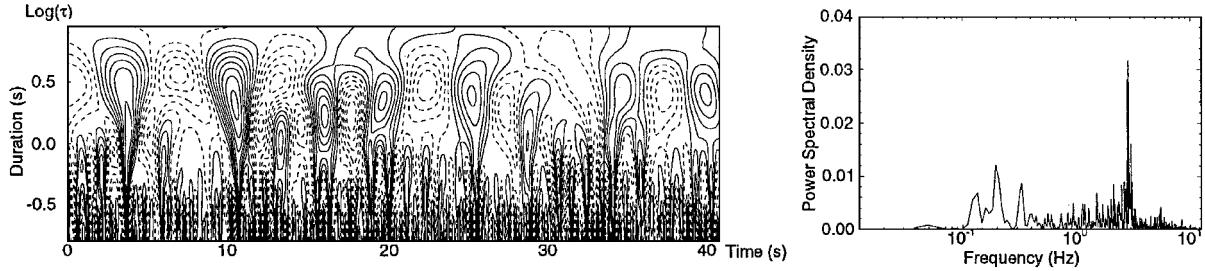

c) $s/h = 1.0, r/D = 0.7$

Fig. 6 Wavelet map and spectral density of axial velocity fluctuations behind three disk models at $x/D = 0.5$.

at a farther downstream station ($x/D = 5.0$) are shown in Fig. 7. In the $s/h = 0.5$ cases, results for the most frequently observed pattern are shown in Figs. 8b and 9b.

At $x/D = 0.5$, power spectral densities behind the slotted disks as well as the solid disk exhibit roughly two frequency ranges (Figs. 6 and 8). The low-frequency peak for the solid disk at 0.1 Hz corresponds to the Strouhal number $Sr = 0.14$ based on disk diameter and freestream velocity. In the wavelet maps on the left, these are indicated by repeated events in the lower two-thirds of each figure along the time axis. In addition, the wavelet maps for the solid disk and $s/h = 0.25$ exhibit very-low-frequency oscillations with 15- to 20-s intervals. The observation of Berger et al.[6] on the solid-disk wake may be recalled here regarding three groups of wake oscillations: the bubble pumping with Strouhal number corresponding to 0.05 based on the diameter, the helical vortex structure with $Sr = 0.135$, and the shear-layer instability with $Sr = 1.62$. Variations of short duration seen near the lower part of the maps correspond to the vortex sheddings from individual annuli as well as instability waves along the main shear layer.

Comparison of the energy distribution between the low-frequency and the high-frequency bands reveals the trend that low-frequency energy decreases as the space ratio increases. The injected momentum indeed appears to suppress the feedback of the downstream low-frequency oscillations, corresponding to both helical and bubble pumping, and shift the energy to higher-frequency range. Further inspection of the wavelet maps indicates that both small- and large-scale structures are intermittent. These irregular, intermittent oscillations resulted in multiple peaks within the low- or high-frequency band in the power spectra. As discussed later, the shape of the low-frequency spectral distributions for individual models is very similar to its downstream counterpart. This suggests that the low-frequency variations at this station are due to the feedback of the dominant wake structures downstream.

In the high-frequency range of the power spectra, the frequency of the spectral peak increases at higher spacing ratios. This also is indicated by decreased intervals between short-duration events. [Compare wavelet maps near $-0.5 < \log(\tau) < 0$, i.e., $0.32\,\text{s} < \tau < 1\,\text{s}$, where τ is the duration or the inverse of the frequency.] Furthermore, the solid-disk wake showed a brief sequence (0–10 s) of strong periodic oscillations, whereas the wavelet maps for the slotted disks showed multiple-scale structures resulting in broadening of spectra. These convoluted structures are due to the Kelvin–Helmholtz instability wave and specific patterns of jet interactions, as well as their relative strengths of jet and outer shear layer. The shedding frequency behind the solid disk is the most concentrated, as noted earlier. For the data corresponding to pattern 3-1-3 in the $s/h = 0.25$ case (Fig. 6b), three jets interact with the main shear layer, causing increased layers of structures in the wavelet map. In comparison, for the $s/h = 0.5$ model (Fig. 8b, pattern 2-3-2) the interactions of two annular jets with the outer shear layer are enhanced because of the larger momentum of the jets. As a result, even wider distribution in shedding frequency was observed. For the $s/h = 1.0$ model (Fig. 6c, pattern 1-5-1), a single strong jet interacts with the main shear layer. The local flow resembles that of a wake flow from a single annulus along the centerline, producing periodic flow concentrated at 2 Hz, a frequency almost twice that for the other s/h ratio.

Figures 7 and 9 compare the velocity fluctuations farther downstream ($x/D = 5$). The spectral peaks are evident approximately at 0.1 Hz and at 0.02 Hz behind the solid disk. In all cases, the overall energy shifted from the small-scale to the large-scale structures downstream. This implies that the shear-layer instability waves and gap vortices have merged and large-scale vortex formations took place between these two stations. The occurrence of large-scale structures [see the wavelet maps around $\log(\tau) = 0.5$] becomes more frequent as the spacing ratio increases. However, the diminished energy level of the very-low-frequency oscillations (in the

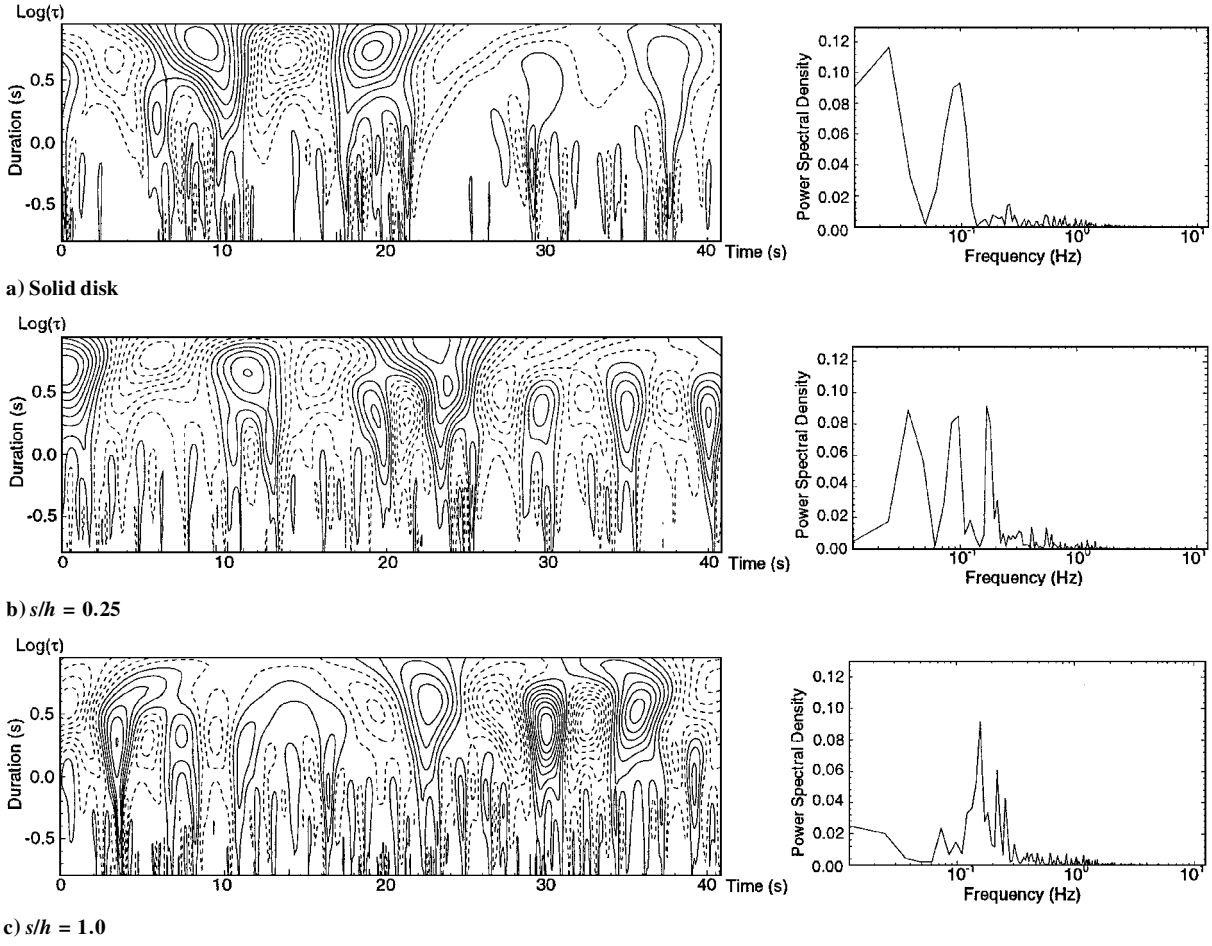

Fig. 7 Wavelet map and spectral density of axial velocity fluctuations behind three disk models at $x/D = 5$, $r/D = 0.7$.

0.01–0.05-Hz range) is clear in the spectral density plots as well as in the wavelet maps. This increasing trend is almost the same as that observed for the small-scale structures upstream, which reflects merged vortices between two stations. The low-frequency peaks in the spectra seen between 0.1 and 0.2 Hz correspond to the large-scale vortex sheddings. As the spacing ratio increases, the peak shifts to a higher frequency while its intensity diminishes, indicating that the injected momentum stabilizes the lateral wake oscillation as well as reduces the size of the wake.

2. Different Patterns

As mentioned earlier, the vortex sheddings of the main shear layer behind different disk models were affected by the flow patterns in the immediate or near-wake region. Therefore, the effect of different flow patterns behind the same model, i.e., identical porosity, is addressed next. Figures 8 and 9 show the wavelet and spectrum of velocity traces at two stations downstream of the $s/h = 0.5$ model.

At $x/D = 0.5$, comparison among wavelet maps and spectra of the three different flow patterns reveals some significant differences in both large- and small-scale structures. Pattern 3-1-3 (Fig. 8a), which has the wake structure similar to that of the solid disk, has the significant energy percentage in the low-frequency band. Focusing our attention on the higher-frequency regime, there is a clear peak at 1 Hz with multiple frequency peaks around it. As shown in the flow visualizations (Fig. 5), the three jets interacted with each other first, and then all together interacted with the main shear layer. The wavelet map of flow pattern 2-3-2 (Fig. 8b) has the most complex small-scale structures, whereas those in the 1-5-1 pattern appear in packets, each having regular intervals. There are no dominant peaks in the spectra, and the wavelet map shows that vortex shedding at different frequency occurred from time to time. In the case of pattern 1-5-1 (Fig. 8c), the significant peaks exist, one at 0.5 Hz, the other at 2 Hz. This indicates interactions between the single outermost jet and the main shear-layer instability wave. These observations are consistent with different patterns of small-scale eddies seen in Fig. 5. Shorter wavelengths are observed in the outer shear layer when a single annular jet is deflected to interact with the outer shear layer (see pattern 1-5-1), and the analysis of the video was consistent with the velocity data. The small-scale structures appear to scale with individual annular element or jet, and an attempt was made to measure the vortex shedding behind each annulus and correlate them with the near-wake flow patttern, but interpretation of the results was arduous without the simultaneous flow visualization and LDV measurements. A study on these spatiotemporal structures with a particle image velocimetry (PIV) has been initiated.

As for the large-scale structures, their energy distribution and energy percentage were different among the patterns. In pattern 2-3-2, the low-frequency energy contribution near 0.1 Hz decreases, and in pattern 1-5-1, it decreases further. The shapes of these low-frequency bands are very similar to those of their downstream counterparts, as discussed later.

At the downstream station ($x/D = 5.0$; Fig. 9), the energy shifted from high-frequency band upstream to low-frequency band regardless of the flow patterns. The energy distribution within the low-frequency bands, however, is different because of the different near-wake patterns. The 1-5-1 pattern has the smallest relative energy content in its low-frequency band compared to the other two patterns. From the wavelet map, the large-scale wake structures appeared irregularly. As more jets remain near the centerline of the wake [from (a) to (c) in Fig. 9], the large-scale structures of the wake become more complex. Naturally, the strength of annular jets also strongly affects the large-scale structure downstream.

IV. Discussion

A. Near-Wake Axisymmetry

Hydrogen bubble visualizations showed the motion of merging jets in the immediate and near-wake regions to be axisymmetric in all cases. This was verified further by visualizing the wake in the cross-

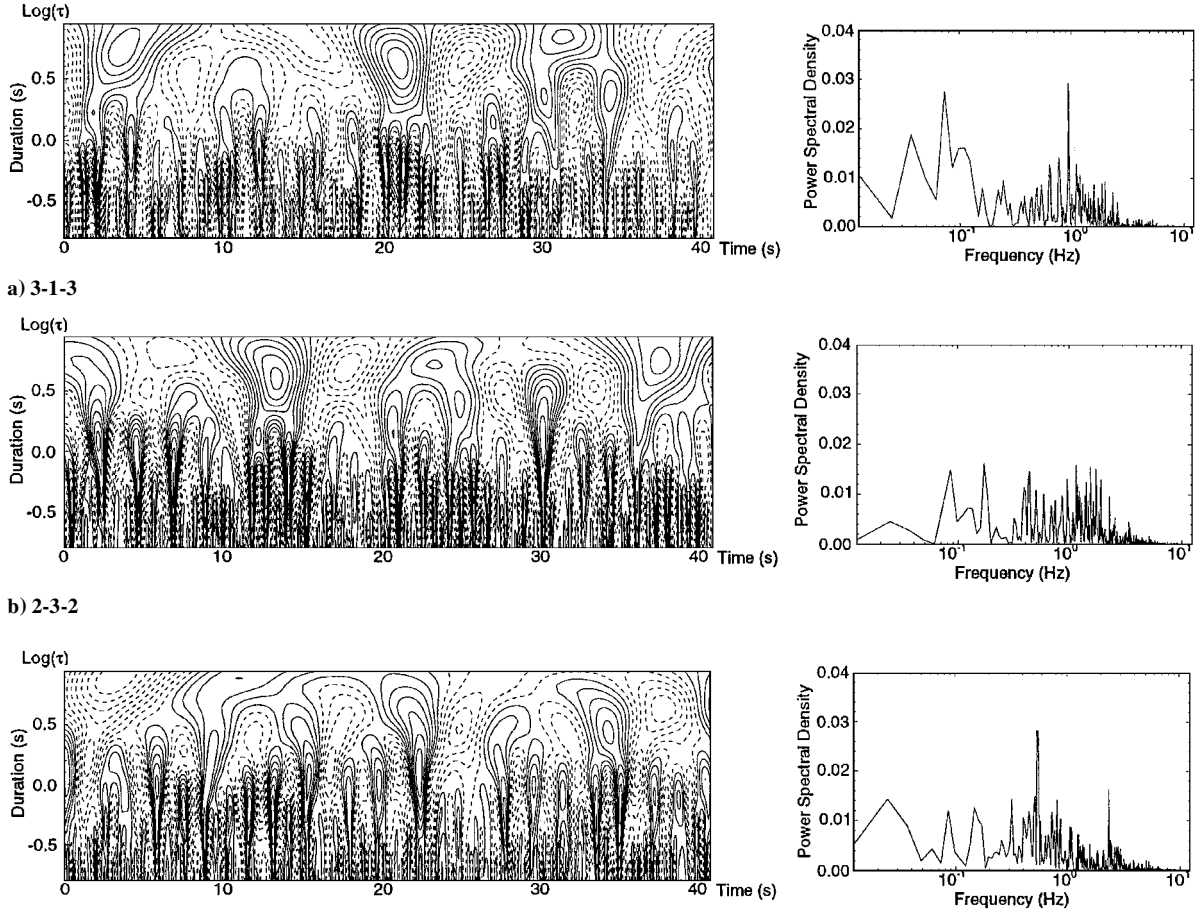

Fig. 8 Wavelet map and spectral density of axial velocity fluctuations behind $s/h = 0.5$ slotted disk at $x/D = 0.5$, $r/D = 0.7$.

sectional plane parallel to the model. The model itself was used as an electrode, and the illumination was provided by the laser sheet. The video depicted axisymmetric wakes of individual rings. Some weak circumferential oscillations also were observed but could not be quantified, whereas slight asymmetry of jet flows occurred only in the $s/h = 0.25$ case. The center jet remained along the axis of the model, and its fluctuations were mostly in the axial direction, as shown by the flow visualization and the radial and axial velocity fluctuation measurements.

In contrast to the preceding findings, the wakes behind two-dimensional models with a similarly large number of slots were found to be asymmetric.[15] The central jet for the two-dimensional $s/h = 0.25$ grid model was deflected on one side and formed a large recirculation downstream. At $s/h = 0.5$, the central jet was always deflected and a number of near-wake patterns were observed, and these wake patterns changed even without external disturbance. A disk with a single center opening also was tested, and its axisymmetric wake pattern was in contrast with biased flow pattern behind a pair of closely spaced flat plates.[10]

According to the present observations, farther downstream up to $x/D = 20$, the wakes behind solid and less porous disks exhibited three-dimensional oscillations, and only the wake behind the most porous case, $s/h = 1.0$ (porosity 43.4%), remained near axisymmetric. The flow visualizations as well as the measurements regarding the absence of dominant large-scale structures are consistent with the findings by Cannon et al.[8] behind axisymmetric screens of various porosity. Their hot-wire measurements and flow visualizations extend much farther downstream than the present study. Those authors also presented modal decompositions of velocity fluctuations at $x/\theta = 105$, where θ is the momentum thickness, and showed a narrow large-scale oscillation of helical $m = \pm 1$ mode at $Sr_\theta = 0.036$ ($Sr = 0.134$ based on the disk diameter) behind the solid disk and much broader and weaker spectral peaks behind the 50% porosity disk at $Sr_\theta = 0.052$ ($Sr = 0.258$) for the $m = \pm 1$ mode.

B. Starting Flow and Specific Wake Pattern

To study how each of the wake patterns gets established, the freestream velocity was ramped up from rest. The time-dependent freestream velocity was found to be repeatable.[16] During the initial startup, all of the jets are parallel to the freestream and free of deflections.

Figure 10a shows the sequence of the startup process for the $s/h = 0.5$ case. Shortly after the initiation of the flow ($t = 2$ s), the incoming flow has moved to the middle of the photograph. The starting vortex can be traced even though the prereleased hydrogen bubbles have started to diffuse out of the focal plane. The velocity through the jets was reduced significantly. The jets remained parallel at $t = 4$ s, where a new ring vortex was about to form along the outer edge of the wake, which can be seen convected downstream at $t = 6$ s. Vortex-induced velocity near the base of the model caused the outward deflection of the jets through outer annular slots. At $t = 8$ s, the flow pattern has already settled into the 3-1-3 pattern. Different relative positions of these starting vortices were observed to form another pattern. When the initial wake vortex formed less distinctly, the outward deflection was limited to the outermost jets, and the jets near the center were deflected toward the jet because of the jet entrainment.

For the $s/h = 0.25$ case, a distinct starting ring vortex formed downstream of the disk edge. The vortex formed closer to the base. Its induced outward velocity, which presumably is higher than that for $s/h = 0.5$, near the base deforms the jets outward. The starting vortex behind a solid disk, which was similar to the present case but more distinctly formed, was reported in Refs. 17 and 18, the latter of which includes the vorticity field in the wake. Figures 10b show the sequence of photographs for the most porous case of spacing ratio, $s/h = 1$. The individual recirculation regions behind the annuli were visible, and so were the starting vortices from the annuli and the center jet. However, the vortex from the disk edge was not as clearly discernible, and individual jets remain nearly parallel to each

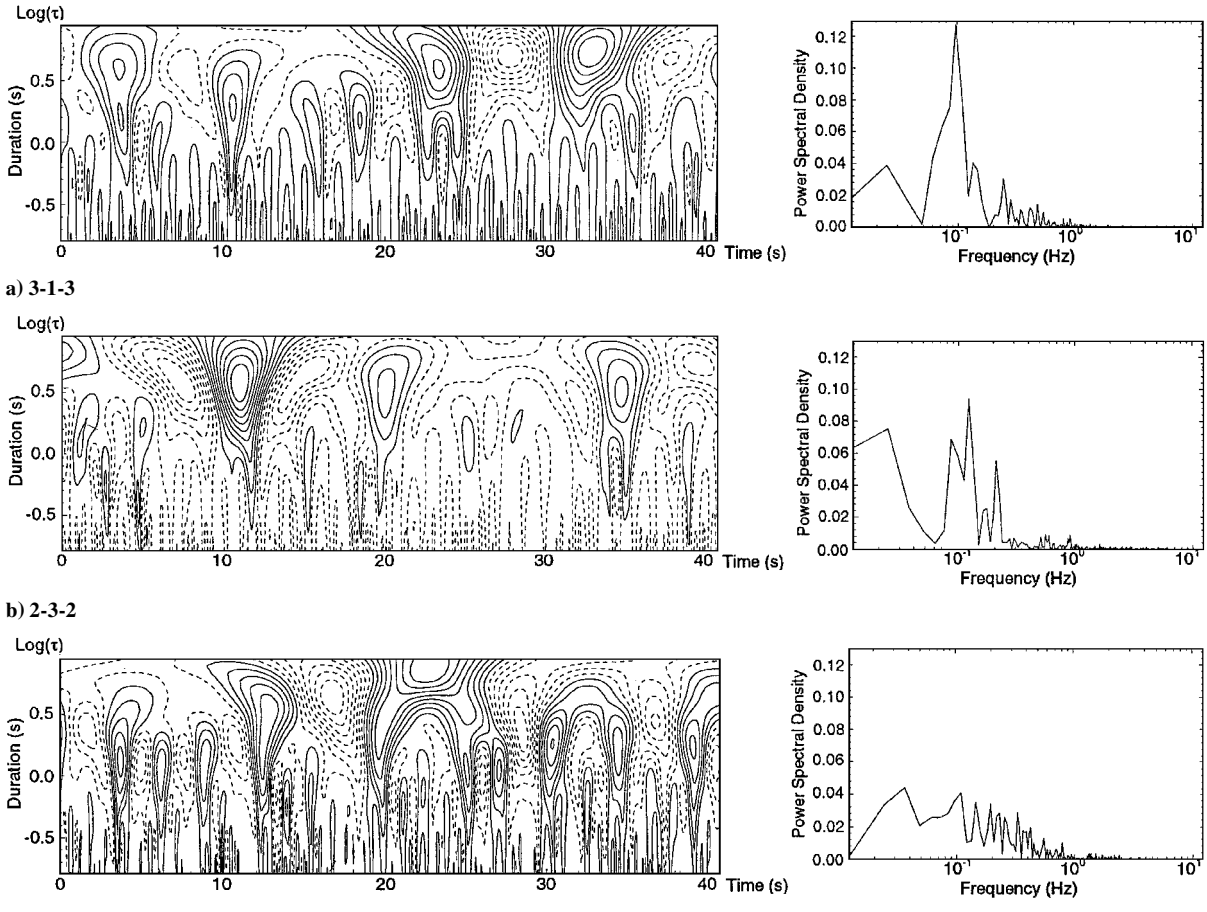

a) 3-1-3

b) 2-3-2

c) 1-5-1

Fig. 9 Wavelet map and spectral density of axial velocity fluctuations behind three disk models at $x/D = 5$, $r/D = 0.7$.

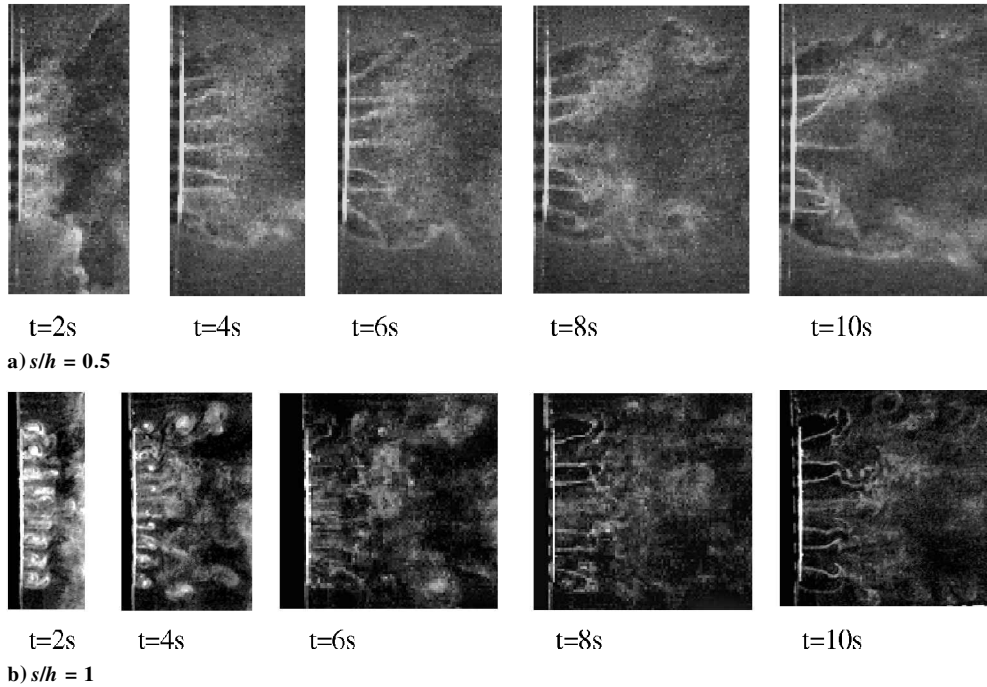

a) $s/h = 0.5$

b) $s/h = 1$

Fig. 10 Starting flow behind $s/h = 0.5$ slotted disk and $s/h = 1$ s.

other. Only the outermost jet was deflected outward because of lower pressure of the flow passing around the disk edge to form the 1-5-1 pattern, which was most frequently observed for this configuration. To further check the role of the jet flow and the outer wake vortex, the center vent was closed, and the flow pattern became predominantly 3-1-3 instead of 1-5-1. More than once, a proto-2-3-2 structure was observed to evolve into a final 3-1-3 in the $s/h = 0.5$ case. Another $s/h = 0.5$ model of a relatively large thickness was tested, and the flow pattern of 1-5-1 was observed more frequently, which was attributable to forced alignment of the jets.

As noted earlier, the center jet remains along the axis, and the near-wake patterns are symmetric, unlike the case in the two-dimensional counterpart. A two-dimensional bluff body may form an asymmetric wake vortex before the final jet mergings are established. The merging pattern was more subject to asymmetric downstream oscillation for the two-dimensional case. The axisymmetric jet merging and

the center jet appear to be prevented from large asymmetric motion topologically unless they produce nutating or swirling motions. Note that there was no mode that produced parallel jet flows. Nonuniform recirculation regions were also observed behind a large number of plates spanning the entire wind-tunnel test section. The normal mass entrainment for the jet flow is suppressed because of the large neighboring recirculation regions in a mechanism similar to biased separation through a large-angle diffuser.

Naturally, the present examples under the specific starting condition cannot be generalized, and other factors, such as excitation to control shear layer instability (see, e.g., Ref. 19), are not considered.

The fact that there were three stages of stable flow patterns and that some large disturbance was required to shift between them suggests a possible theoretical explanation of the behavior, either an energy-based stability argument or a nonlinear bifurcation theory. Such argument already has been made to similar but somewhat simpler two-dimensional configurations.[20]

V. Conclusion

Interactions of jets and their effects on the wake behavior were studied experimentally behind the slotted disks at different spacing ratios. Jets through individual slots merged in a multiply stable, axisymmetric manner in both mean flow and time-dependent flows. The intermediate wake was dominated by three-dimensional large-scale motions for small spacing ratios. Onset of the specific flow patterns is believed to be associated with the interactions among startup vortices. Although these interactions are smoothed out farther downstream, the precise merging patterns and force exerted on the individual annuli are critical in some engineering problems such as the inflation process of ribbon parachutes. Measurements with PIV have been initiated to address some of the issues raised.[21]

Acknowledgments

The present work was supported partly by the U.S. Naval Air Warfare Center, Mitsubishi Heavy Industries, and the National Science Foundation REU Program. Reviewers' comments are gratefully acknowledged.

References

[1]Huerre, P., and Monkewitz, P. A., "Local and Global Instabilities in Spatially Developing Flows," *Annual Review of Fluid Mechanics*, Vol. 22, 1990, pp. 473–537.

[2]Huang, Z., and Keffer, J. F., "Development of Structure Within the Turbulent Wake of a Porous Body, Part 1: The Initial Formation Region," *Journal of Fluid Mechanics*, Vol. 329, 1996, pp. 103–115.

[3]Huang, Z., Kawall, J. G., and Keffer, J. F., "Development of Structure Within the Turbulent Wake of a Porous Body, Part 2: Evolution of the Three-Dimensional Features," *Journal of Fluid Mechanics*, Vol. 329, 1996, pp. 117–136.

[4]Peterson, C. W., Strickland, J. H., and Higuchi, H., "The Fluid Dynamics of Parachute Inflation," *Annual Review of Fluid Mechanics*, Vol. 28, 1996, pp. 361–387.

[5]Fuchs, H. V., Mercker, E., and Michel, U., "Large-Scale Coherent Structures in the Wake of Axisymmetric Bodies," *Journal of Fluid Mechanics*, Vol. 93, Pt. 1, 1979, pp. 185–207.

[6]Berger, E., Scholtz, D., and Schumm, M., "Coherent Vortex Structures in the Wake of a Sphere and a Circular Disk at Rest and Under Forced Vibrations," *Journal of Fluids and Structures*, Vol. 4, 1990, pp. 231–257.

[7]Bevilaqua, P. M., and Lykoudis, P. S., "Turbulence Memory in Self-Preserving Wakes," *Journal of Fluid Mechanics*, Vol. 89, Pt. 3, 1978, pp. 589–606.

[8]Cannon, S., Champagne, F., and Glezer, A., "Observations of Large-Scale Structures Behind Axisymmetric Bodies," *Experiments in Fluids*, Vol. 14, No. 6, 1993, pp. 447–450.

[9]Roberts, B. W., "Drag and Pressure Distribution on a Family of Porous, Slotted Disks," *Journal of Aircraft*, Vol. 17, No. 6, 1980, pp. 393–401.

[10]Higuchi, H., Lewalle, J., and Crane, P., "On the Structures of a Two-Dimensional Wake Behind a Pair of Flat Plates," *Physics of Fluids*, Vol. 6, No. 1, 1994, pp. 297–305.

[11]Bearman, P. W., and Takamoto, M., "Vortex Shedding Behind Rings and Disks," *Fluid Dynamics Research*, North-Holland, Amsterdam, 1988, pp. 214–218.

[12]Leweke, T., and Provansal, M., "The Flow Behind Rings: Bluff Body Wakes Without End Effects," *Journal of Fluid Mechanics*, Vol. 288, 1995, pp. 265–310.

[13]Hayashi, M., Sakurai, A., and Ohya, Y., "Wake Interference of a Row of Normal Flat Plates Arranged Side by Side in a Uniform Flow," *Journal of Fluid Mechanics*, Vol. 164, March 1986, pp. 1–25.

[14]Higuchi, H., "Experimental Investigation of the Flowfield Behind Grid Models," *Journal of Aircraft*, Vol. 26, No. 4, 1989, pp. 308–314.

[15]Higuchi, H., and Takahashi, F., "Flow Past Two-Dimensional Ribbon Parachute Models," *Journal of Aircraft*, Vol. 26, No. 7, 1989, pp. 641–649.

[16]Higuchi, H., Anderson, R. W., and Zhang, J., "Three-Dimensional Wake Formations Behind Regular Polygonal Plates," *AIAA Journal*, Vol. 34, No. 6, 1996, pp. 1138–1145.

[17]Higuchi, H., Balligand, H., and Strickland, J. H., "Numerical and Experimental Investigations of the Flow over a Disk Undergoing Unsteady Motion," *Journal of Fluids and Structures*, Vol. 10, No. 7, 1996, pp. 705–719.

[18]Balligand, H., Zhang, J., and Higuchi, H., "Wake Structure Behind a Disk Started in Uniform and Near-Impulsive Accelerations," American Society of Mechanical Engineers, Fluids Engineering Div. Summer Meeting, FEDSM 98-5163, Washington, DC, June 1998.

[19]Kim, H. J., and Durbin, P. A., "Investigation of the Flow Between a Pair of Circular Cylinders in the Flopping Regime," *Journal of Fluid Mechanics*, Vol. 196, 1988, pp. 431–448.

[20]Chauve, M. P., and Le Gal, P., "Complex Bi-Orthogonal Decomposition of a Chain of Coupled Wakes," *Physica D: Nonlinear Phenomena*, Vol. 58, Nos. 1/4, 1992, pp. 407–413.

[21]Higuchi, H., Zhang, J., and Balligand, H., "Particle Image and Dye Flow Visualization Behind Solid and Slotted Disks in Unsteady Motions," 8th International Symposium on Flow Visualization, Sorrento, Italy, Sept. 1998.

A. Plotkin
Associate Editor